

PCCP

Accepted Manuscript



This is an *Accepted Manuscript*, which has been through the Royal Society of Chemistry peer review process and has been accepted for publication.

Accepted Manuscripts are published online shortly after acceptance, before technical editing, formatting and proof reading. Using this free service, authors can make their results available to the community, in citable form, before we publish the edited article. We will replace this *Accepted Manuscript* with the edited and formatted *Advance Article* as soon as it is available.

You can find more information about *Accepted Manuscripts* in the [Information for Authors](#).

Please note that technical editing may introduce minor changes to the text and/or graphics, which may alter content. The journal's standard [Terms & Conditions](#) and the [Ethical guidelines](#) still apply. In no event shall the Royal Society of Chemistry be held responsible for any errors or omissions in this *Accepted Manuscript* or any consequences arising from the use of any information it contains.

Thermal Relaxation of Lithium Dendrites

Asghar Aryanfar^{1*}, Daniel J. Brooks², Boris V. Merinov², William A. Goddard III², Agustin J. Colussi^{1*} and Michael R. Hoffmann¹

¹Linde Center for Global Environmental Science; ²Materials & Process Simulation Center, California Institute of Technology, Pasadena, CA 91125, U.S.A.

CP-ART-12-2014-005786-R1

* Corresponding Authors: AA: aryanfar@caltech.edu, AJC: ajcoluss@caltech.edu

ABSTRACT

The average lengths $\bar{\lambda}$ of lithium dendrites produced by charging symmetric Li^0 batteries at various temperatures are matched by Monte Carlo computations dealing both with Li^+ transport in the electrolyte and thermal relaxation of Li^0 electrodeposits. We found that experimental $\bar{\lambda}(T)$ variations cannot be solely accounted by the temperature dependence of Li^+ mobility in the solvent but require the involvement of competitive Li-atom transport from metastable dendrite tips to smoother domains over $\Delta E_R^\ddagger \sim 20 \text{ kJ mol}^{-1}$ barriers. A transition state theory analysis of Li-atom diffusion in solids yields a negative entropy of activation for the relaxation process: $\Delta S_R^\ddagger \approx -46 \text{ J mol}^{-1} \text{ K}^{-1}$ that is consistent with the transformation of amorphous into crystalline Li^0 electrodeposits. Significantly, our $\Delta E_R^\ddagger \sim 20 \text{ kJ mol}^{-1}$ value compares favorably with the activation barriers recently derived from DFT calculations for self-diffusion on Li^0 (001) and (111) crystal surfaces. Our findings suggest a key role for the mobility of interfacial Li-atoms in determining the morphology of dendrites at temperatures above the onset of surface reconstruction: $T_{\text{SR}} \approx 0.65 T_{\text{MB}}$ ($T_{\text{MB}} = 453 \text{ K}$ is the melting point of bulk Li^0).

INTRODUCTION

Portable electronic devices and intermittent renewable energy sources demand high-capacity, reliable, long-lasting electric energy storage units.¹⁻³ The low mass density (0.564 g cm^{-3}) and high reduction potential ($E^0 = -3.04 \text{ V vs. SHE}$) of lithium metal (Li^0) should make it the ideal electrode material.⁴⁻⁸ Li^0 , however, is exceptionally prone to grow dendrites under the far from equilibrium conditions prevalent during electrodeposition.^{4, 9-15} The runaway growth of metallic dendrites is the harbinger of short-circuiting, overheating, and ultimately the ignition of the organic solvents used in Li^0 batteries.¹⁶ Intense efforts are therefore underway to prevent such hazards by limiting dendrite growth during battery charging.¹⁶⁻¹⁹

At present, efforts aimed at controlling Li^0 dendrite growth remain semi-empirical because its mechanism is not fully understood.¹⁹⁻³³ Models fall short of capturing the complex dynamics of dendrite inception and growth,^{21, 34, 35} or accounting for the peculiar facility of Li^0 to grow dendrites relative to other potentially useful 1st- and 2nd-period metals.³⁶⁻⁴⁵ In our view, control strategies should consider that dendrite growth is a non-deterministic stochastic process,⁴⁶⁻⁵¹ and the propensity of Li^0 for growing dendrites a direct consequence of the inherent Li-Li binding energy and energy barrier values for Li-atom transport on the metal surface.⁵²⁻⁵⁴ We have previously addressed the former issue via pulsed charging experiments and Monte Carlo computations.⁴⁶ Here we report experiments and computations aimed at quantifying the thermal behavior of electrolytic Li^0 dendrites as a first step toward linking Li^0 properties with dendrites growth and control.⁵⁵⁻⁵⁷

Our experiments consist of charging symmetric coin Li^0 batteries that allow for *in situ* visualization of dendrites.⁵⁸⁻⁶⁰ Disk electrodes (area = 1.6 cm^2) punched from cleaned Li^0 foil (Aldrich, 99.9%, 0.38 mm thick, were mounted $L = 3.175 \text{ mm}$ apart on an open-ended transparent polymethyl-methacrylate (PMMA) cylindrical tube separator. The electrolyte was a 1 M LiClO_4 (Aldrich, battery grade, 99.99%, dried for 24 hours at $90 \text{ }^\circ\text{C}$ under vacuum) solution in propylene carbonate (PC) (Aldrich, 99.7% Anhydrous). Batteries were submerged in a

thermostated bath as shown in Fig. 1, and charged galvanostatically at 2 mA cm^{-2} for 8 or 24 hours in a glovebox sparged with argon (H_2O , $\text{O}_2 < 0.5 \text{ ppm}$). We estimated that (1) convection is negligible in our experiments since the value of the Rayleigh number $\text{Ra} = 1708$ at which convection sets in our system is estimated to be reached in layers of thickness $\delta > 10 \text{ }\mu\text{m}$ (i.e., in the bulk electrolyte) that exceed the thickness of the electrochemical double layer where the relevant processes take place,⁶¹ (2) linear temperature gradients normal to the cathode are established within minutes (see Supplementary Information), (3) the limiting diffusional current density for discharging Li^+ in PC: $J \gg D C_0/L = 78 \text{ mA/cm}^2$ is much larger than the 1 mA/cm^2 value used in our experiments.⁶²

After charging, batteries were removed from the glovebox for the acquisition of high-resolution digital images of the electrodeposits with a Leica 205FA microscope. The digital images of the three equiangular 120° sectors of the curved peripheries of the cylindrical cells were then projected onto a flat surface as described in our previous publication.⁵⁹ Forty five equidistant dendrites were selected from the projected images and sorted into $[n_i, \lambda_i]$ bins within specified length ranges λ_i . From this information we evaluated normalized average lengths, $\bar{\lambda}$, defined by equation E1:

$$\bar{\lambda} = \frac{\int n_i \lambda_i}{L \int n_i} \quad (\text{E1})$$

that properly quantify the growth of dendrite populations generated by a stochastic process. The experimental $[n_i, \lambda_i]$ distributions are shown in Fig. 2. Fig. 3 shows plots of average lengths $\bar{\lambda}$ versus cathode temperature T .

Model calculations were based on our recently developed coarse-grained dynamical Monte Carlo (CG-MC) framework.^{46, 63} The core 2D CG-MC algorithm calculates the combined diffusional and migrational Li^+ displacements using temperature dependent Li^+ diffusion coefficients, $D_+(T)$, and mobilities, $\mu_+(T)$, under local electric $\vec{E}(x, y, t)$ and temperature $T(x, y, t)$

fields (x and y are the parallel and perpendicular coordinates to electrodes surfaces) (see below). $D_+(T)$ is assumed to follow an Arrhenius temperature dependence, equation E2:

$$D_+(T) = D_+^0 \exp(-E_\eta/Nk_B T) \quad (\text{E2})$$

From which we evaluate $\mu_+(T)$ by using the Stokes-Einstein relation, equation E3:

$$\mu_+(T) = \frac{e D_+(T)}{Nk_B T} \quad (\text{E3})$$

k_B is Boltzmann's constant, N is Avogadro's number, e the elementary charge, and $E_\eta = 13.5$ kJ mol⁻¹ the experimental activation energy derived from viscosity $\eta(T)$ data for the PC solvent (Table 1). Temperature $T(x,y,t)$ and electric field $\vec{E}(x,y,t)$ profiles were evaluated by finite-differences integration of the corresponding 2D Laplace's equations as described in our recent publication (See Supplementary Information for details).⁴⁶ The surface of electrodeposits was set at T_+ and V_- throughout, on account of the high Li^0 electrical and thermal conductivities. CG-MC simulations were run in a $[L^* \times L^*]$, $L^* = 16.7$ nm, domain that approximately corresponds to the thickness of the depletion layers where the relevant events take place in this system (see Table 1). It is important to note that the actual $D_+(T)$ value used in the calculations was scaled down from experimental values ($D_+^{\text{exp}}(300 \text{ K}) = 2.58 \times 10^{-6} \text{ cm}^2 \text{ s}^{-1}$)⁶² for Li^+ diffusion in PC to yield diffusional displacements $\langle x^2 \rangle^{1/2} \approx L^*/2$ at the end of simulations. The rationale for such scaling has been described in a previous publication from our laboratory.⁴⁶ Since the $\Delta t = 0.25 \mu\text{s}$ simulation time-step is much longer than the ps time-scale of ion-ion collisions, Li^+ ions positions $\vec{r}_i(t)$ were computed from average displacements given by equation E4:

$$\vec{r}_i(t + \Delta t) = \vec{r}_i(t) + \sqrt{2 D_+(T) \Delta t} \vec{g} + \mu_+(T) \vec{E}(\vec{r}, t) \Delta t \quad (\text{E4})$$

where \vec{g} is a random unit vector, and $\vec{E}(\vec{r}, t)$ is the position and time dependent electric field vector. The voltage drop across the $[16.7 \text{ nm} \times 16.7 \text{ nm}]$ domain: $V_+ - V_- = 47$ mV, is scaled to generate the $\approx 10^4 \text{ V cm}^{-1}$ electric fields that make ion electromigration competitive with diffusion.^{34, 46} We further assumed that Li^+ is reduced to Li^0 with temperature-independent unit

probability under the applied overpotentials. The actual parameters used in the simulations are listed in Table 1 (see below). Further details can be found in our previous publication.⁴⁶

Since dendrites tips are intrinsically metastable formations possessing excess surface free energy relative to flat Li^0 crystals,^{64, 65} they should eventually relax at appreciable rates via Li^0 -atom diffusion into interfacial sites of lower curvature/higher connectivity at sufficiently high temperatures.^{66, 67} This relaxation process was incorporated into our model calculations by releasing Li^0 atoms with probabilities $p_R(T)$ given by equation E5:⁶⁶

$$p_R(T) = p_R^0 \exp\left(\frac{-\Delta E_R^\ddagger}{Nk_B T}\right) \quad (\text{E5})$$

p_R^0 is an adjustable dimensionless pre-factor and ΔE_R^\ddagger is the effective activation energy for Li-atom hopping on our dendritic electrodeposits. The pre-factor was selected such that relaxation rates were competitive with deposition rates. We found that the temperature dependence of the $\bar{\lambda}(T)$ calculated in this manner was not overly sensitive to the value of the pre-factor, as long as the above condition was satisfied. At each integration step, Li^0 atoms are released into the electrolyte as Li^+ ions at distances $4r_+$ ($r_+ = 1.19 \text{ \AA}$ is Li^+ crystalline radius) away from the nearest surface Li^0 atoms, which then evolve according to (E3). Each interfacial Li^0 -atom undergoes on average 4-5 rearrangements per simulation. The dissolution of Li^0 into Li^+ in close proximity of deposits followed by re-deposition is operationally equivalent to the diffusion of Li^0 atoms from dendrite tips to concave regions. This is so because Li^+ ions released from dendrite tips have fewer neighboring surface sites to which return as Li^0 than those released from concave cathode regions. Simulations were stopped the first time 400 Li^0 appeared the system. The total number of Li^+ ions was preserved by creating a new Li^+ at a random location whenever another Li^+ was annihilated as Li^0 . Calculated dendrite heights were quantified by dividing the x-axis in four sectors. Here, 'dendrite height' in each sector is the height of the uppermost Li^0 defined by equation E6:

$$\lambda_i = \max_{k=1:n} \xi_k \cdot \mathbf{j} \quad (\text{E6})$$

where λ_i is dendrite height, $\vec{\xi}_k$ the individual atoms coordinates in sector i , n is the total number of lithium atoms incorporated into the dendrite in the corresponding sector and \mathbf{j} is the unit vector in y direction. To ensure good statistics, each simulation was run 10 times. From this information we evaluated $\bar{\lambda}$ values for comparison with experimental ones. Fig. 4 shows typical snapshots of calculated dendrites at three T values. In Fig. 5 computational $\bar{\lambda}$ values calculated by excluding and including surface relaxation are compared with experimental $\bar{\lambda}$ ones.

Our experimental results show that keeping the cathode warmer than the surrounding solution does inhibit dendrite growth. We have recently shown that the positive feedback underlying runaway dendrite growth is due to the fact that Li^+ electromigration in the strong electric fields developing around high- curvature dendrite tips outpaces Li^+ diffusion to flatter regions.⁵⁸ Since D_+ and μ_+ increase exponentially with T , and the electrolyte filling concave pockets is significantly warmer than the layers surrounding dendrite tips (Fig. S1), we expected that the application of negative temperature gradients to the cathode would enhance diffusional-limited current densities to concave regions relative to dendrite tips. In other words, we expected that model simulations of the relatively faster Li^+ electrodeposition on cathode regions surrounded by warmer electrolyte layers would account for our experimental findings.

The results of GC-MC simulations (Fig. 5) dispelled our simplistic expectations. The reasons are that the $D_+(T)$, $\mu_+(T)$ dependences originating from $E_{\eta} = 13.5 \text{ kJ mol}^{-1}$ (Table 1) are not only halved into diffusional $\bar{\lambda}(T)$ displacements, but they are also attenuated by the competition between ion diffusion and electromigration in the non-linear $T(x,y,t)$, $\vec{E}(x,y,t)$ and $[\text{Li}^+(x,y,t)]$ fields surrounding the irregular Li^0 deposits (Fig. 4). Thus, the results of Fig. 5 in effect implicate the participation of a process having a stronger temperature dependence than that associated with Li^+ transport in the electrolyte solvent. Thus, we found that we could match the experimental $\bar{\lambda}(T)$ temperature trends by including the thermal relaxation of Li^0 dendrites, as simulated by the process described above, with $\Delta E_R^{\ddagger} \approx 20 \text{ kJ mol}^{-1}$. The possibility that the

formation of an insulating solid-electrolyte interfacial layer (SEI) could be responsible for our observations in apparently negated by the fully reversible galvanostatic curves we previously registered in this system upon successive charge/discharge cycles.⁵⁹

A transition state theory (TST) analysis of atom diffusion in metallic solids provides a physical interpretation of our findings.⁶⁸⁻⁷⁰ The TST expression for the diffusion coefficient D_{TST} of Li-atoms on the surface of Li^0 metal is given by equation (E7):⁵⁴

$$D_{TST} = (1/4) a^2 \frac{k_B T}{h} \exp \frac{\Delta S^*}{Nk_B} \exp \left(-\frac{\Delta E^*}{Nk_B T} \right) = D_{TST}^0 \exp \left(-\frac{\Delta E^*}{Nk_B T} \right) \quad (\text{E7})$$

where $a = 3.49 \text{ \AA}$ is the lattice constant,⁵² h is Planck's constant, and ΔS^* , ΔE^* are the activation entropy and enthalpy of the process. Thus: $D_{TST} \approx 2 \times 10^{-3} \text{ cm}^2 \text{ s}^{-1} \exp \frac{\Delta S^*}{Nk_B} \exp \left(-\frac{\Delta E^*}{Nk_B T} \right)$ at $T_{1/2} = 318 \text{ K}$, the mean temperature in our experiments. By assuming that the shortening of dendrites at higher temperatures is due to Li-atom diffusion from dendrite tips to sites of higher coordination, we interpret that relative $\overline{\Delta \lambda(T)} = \langle x^2 \rangle_T^{1/2} - \langle x^2 \rangle_{T=21^\circ\text{C}}^{1/2}$ experimental decrements (from Fig. 2a) correspond in fact to average Li-atom diffusional displacements on the surface of dendrites. On this basis, from $D_{exp} = \overline{\Delta \lambda}^2 (2\tau)^{-1}$, $\tau = 8 \text{ h}$, we estimate an average experimental diffusion coefficient $D_{exp} \approx 9 \times 10^{-8} \text{ cm}^2 \text{ s}^{-1}$ at $T_{1/2}$. By identifying D_{TST} with D_{exp} , and ΔE_R^\ddagger with ΔE^* we derive a pre-factor $D_{TST}^0 = 4 \times 10^{-5} \text{ cm}^2 \text{ s}^{-1}$ that is in the range of those typical for atom self-diffusion on metal surfaces,⁷¹⁻⁷³ and leads to a significant negative entropy of activation: $\Delta S^* = -46 \text{ J mol}^{-1} \text{ K}^{-1}$, consistent with the transformation of (disordered) amorphous Li^0 dendrites into Li^0 crystals.^{74, 75} Gratifyingly, the $\Delta E^* = 20 \text{ kJ mol}^{-1}$ value derived from our experiments and CG-MC calculations falls within the range of the DFT values for the activation barriers of Li-atom hopping and exchange on $\text{Li}(001)$ and $\text{Li}(111)$ single crystals.⁵² The type of surface reconstruction we observe for metallic lithium dendrites above ambient temperatures is a universal phenomenon.⁶⁶ For a melting point of bulk Li^0 : $T_{MB} = 180 \text{ }^\circ\text{C} = 453 \text{ K}$, the condition $T/T_{MB} > 0.7$ that determines the onset of surface reconstruction is already met by Li^0 at ≈ 300

K.⁶⁶ The above condition, which strictly applies to flat Li^0 crystals, will be relaxed for microcrystalline dendrites because the melting point T_{MD} of dendrite tips of radius of curvature ρ is necessarily lower than T_{MB} . From the Gibbs-Thompson equation that relates T_{MD} with T_{MB} , E8:⁷⁶⁻⁷⁸

$$T_{MD} = T_{MB} \left(1 - \frac{4 \sigma_{SL}}{\Delta H_{MB} d_S \rho} \right) \quad (\text{E8})$$

with solid-liquid surface energy $\sigma_{SL} = 0.41 \text{ J m}^{-2}$,^{79, 80} melting enthalpy $\Delta H_{MB} = 512 \text{ KJ Kg}^{-1}$, and solid density $d_S = 430 \text{ Kg m}^{-3}$, we estimate that, for example, the T_{MD} of conceivable dendrite tips sharper than $\rho < 73 \text{ nm}$ would be: $T_{MD} < 0.9 T_{MB} \approx 400 \text{ K} = 127 \text{ }^\circ\text{C}$.

Summing up, our experiments and calculations open up the possibility that the runaway growth of electrolytic Li^0 dendrites could be better controlled by increasing the mobility of Li-atoms on the solid than by increasing the mobility of Li^+ ions in the electrolyte. They also suggest specific approaches, such as enhancing interfacial Li-atom diffusion by implanting extrinsic defects.^{70, 81-85}

ACKNOWLEDGMENTS

Authors gratefully acknowledge support from the Bill and Melinda Gates Foundation Grant No. OPP1069500 on environmental sustainability and, in part, from Bosch Energy Research Network Grant No. 13.01.CC11.

Table 1 –Parameters used in CG-MC calculations

Domain size	$L^* \times L^* = (17 \times 17) \text{ nm}^2$
V_+	0 V
V_-	- 47 mV
D_+^0	$3.4 \times 10^{-8} \text{ cm}^2 \text{ s}^{-1}$
r_+	1.19 Å
E_η	13.5 kJ mol ⁻¹
ΔE_R^\ddagger	20 kJ mol ⁻¹
p_R^0	300

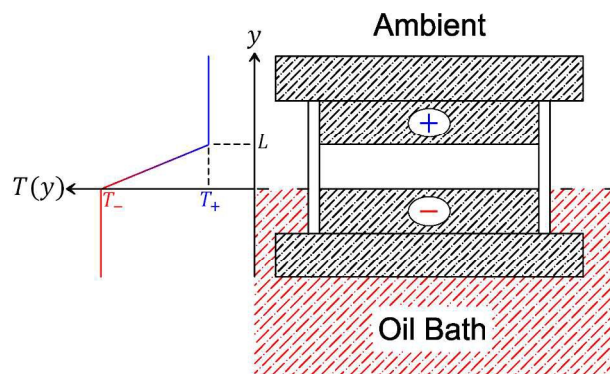


Figure 1 - Schematic diagram of the experiment setup. The initial steady-state temperature profile is shown on the left. See text.

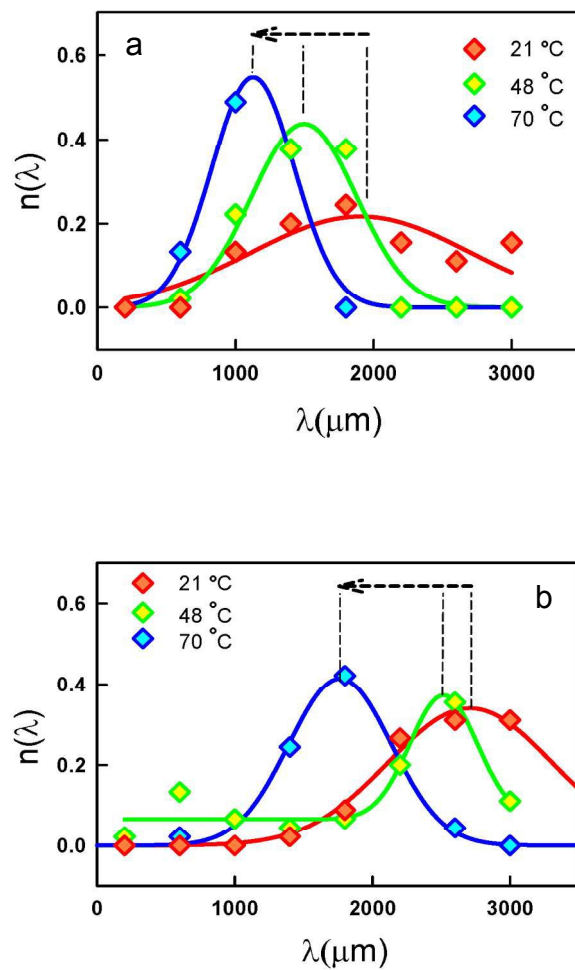


Figure 2 – Normalized dendrite length distributions $[n_i, \lambda_i]$ at various cathode temperatures T_- . Cells charged at 2 mA cm^{-2} for (a) 8 h, (b) 24 h.

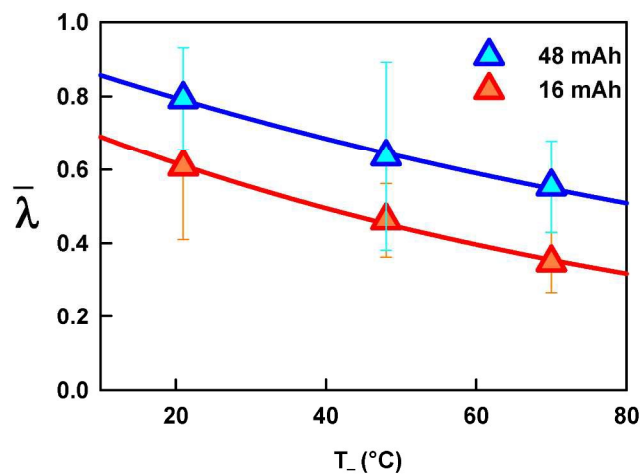


Figure 3 - Average dendrite lengths $\bar{\lambda}$ as fractions of interelectrode separation L versus cathode temperature $T_$.

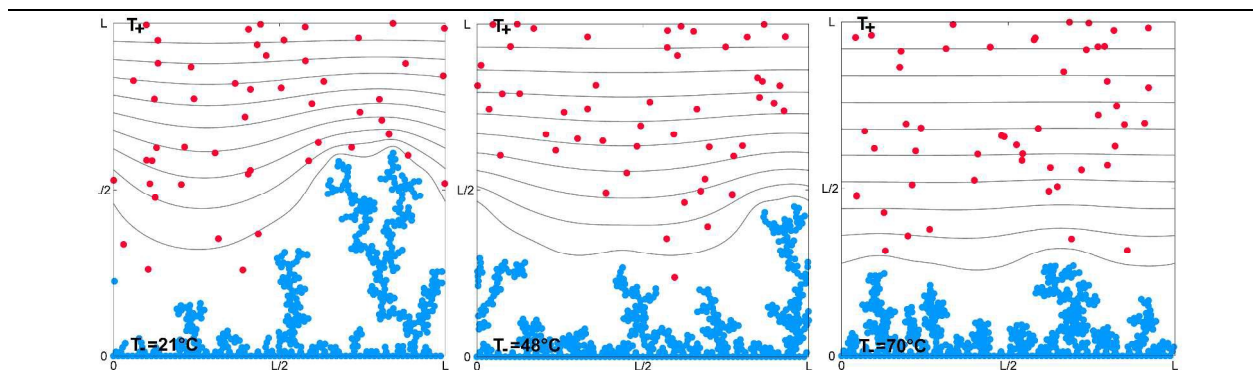


Figure 4 – Results of CG-MC calculations including both Li⁺ transport and Li⁰ thermal relaxation (see text). Blue dots: Li⁰ in dendrites. Red dots: Li⁺ ions in solution. Gray lines are isotherms. From left to right, results at T. = 21°, 48° and 70°C.

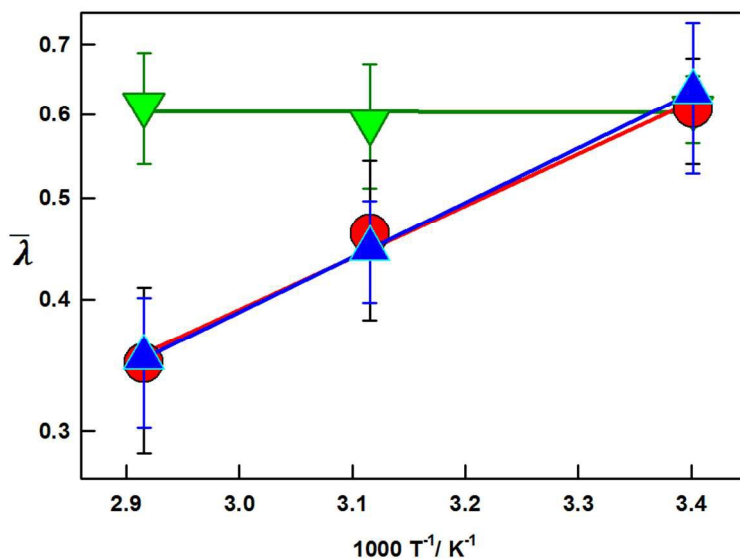
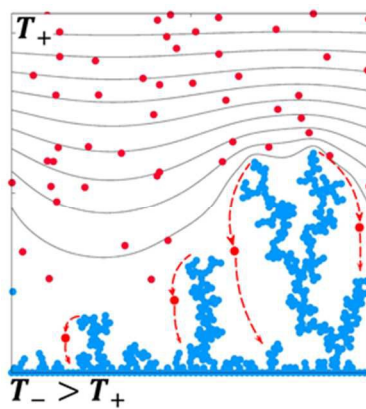


Figure 5 - Arrhenius $\log \bar{\lambda}$ vs. $1/T$ plots. Red circles: experimental $\bar{\lambda}$ data obtained at 16 mAh (Fig. 2a); Green downward triangles: simulated $\bar{\lambda}$ by excluding dendrites relaxation. Blue upward triangles: simulated $\bar{\lambda}$ by including dendrites relaxation. Lines are linear regressions to the data. Simulated data (green and blue points) pinned to the experimental value (red) at 21°C to help visualize slope differences.

REFERENCES

1. J. Rugolo and M. J. Aziz, *Energy & Environ. Sci.*, 2012, 5, 7151-7160.
2. M. Armand and J. M. Tarascon, *Nature*, 2008, 451, 652-657.
3. B. Dunn, H. Kamath and J.-M. Tarascon, *Science*, 2011, 334, 928-935.
4. W. Xu, J. L. Wang, F. Ding, X. L. Chen, E. Nasybutin, Y. H. Zhang and J. G. Zhang, *Energy & Environ. Sci.*, 2014, 7, 513-537.
5. H. Kim, G. Jeong, Y. U. Kim, J. H. Kim, C. M. Park and H. J. Sohn, *Chem. Soc. Rev.*, 2013, 42, 9011-9034.
6. J. M. Tarascon and M. Armand, *Nature*, 2001, 414, 359-367.
7. J. B. Goodenough, *Acc. Chem. Res.*, 2012.
8. J. B. Goodenough, *J. Solid State Electrochem.*, 2012, 16, 2019-2029.
9. K. J. Harry, D. T. Hallinan, D. Y. Parkinson, A. A. MacDowell and N. P. Balsara, *Nature Mat.*, 2014, 13, 69-73.
10. R. L. Sacci, N. J. Dudney, K. L. More, L. R. Parent, I. Arslan, N. D. Browning and R. R. Unocic, *Chem. Comm.*, 2014, 50, 2104-2107.
11. C. M. Lopez, J. T. Vaughey and D. W. Dees, *J. Electrochem. Soc.*, 2009, 156, A726-A729.
12. H. Liu, F. C. Strobridge, O. J. Borkiewicz, K. M. Wiaderek, K. W. Chapman, P. J. Chupas and C. P. Grey, *Science*, 2014, 344.
13. T. R. Ferguson and M. Z. Bazant, *Electrochim. Acta*, 2014, 146, 89-97.
14. J. Owen and A. Hector, *Science*, 2014, 344, 1451-1452.
15. M. S. Whittingham, *Chemical Reviews*, 2014, 114, 11414-11443.
16. K. Xu, *Chem. Rev.*, 2004, 104, 4303-4418.
17. J. Steiger, D. Kramer and R. Monig, *J. Power Sources*, 2014, 261, 112-119.
18. Y. Y. Lu, Z. Y. Tu and L. A. Archer, *Nat. Mat.*, 2014, 13, 961-969.
19. M. Z. Mayers, J. W. Kaminski and T. F. Miller III, *J. Phys. Chem. C*, 2012, 116, 26214-26221.
20. J. L. Barton and J. O. M. Bockris, *Proc. Royal Soc. London. Series A*, 1962, 268, 485-505.
21. C. Monroe and J. Newman, *J. Electrochem. Soc.*, 2003, 150, A1377-A1384.
22. P. C. Howlett, D. R. MacFarlane and A. F. Hollenkamp, *J. Power Sources*, 2003, 114, 277-284.
23. N. Schweikert, A. Hofmann, M. Schulz, M. Scheuermann, S. T. Boles, T. Hanemann, H. Hahn and S. Indris, *J. Power Sources*, 2013, 228, 237-243.
24. O. Crowther and A. C. West, *J. Electrochem. Soc.*, 2008, 155, A806-A811.
25. C. Brissot, M. Rosso, J. N. Chazalviel, P. Baudry and S. Lascaud, *Electrochim. Acta*, 1998, 43, 1569-1574.
26. I. W. Seong, C. H. Hong, B. K. Kim and W. Y. Yoon, *J. Power Sources*, 2008, 178, 769-773.
27. G. Stone, S. Mullin, A. Teran, D. Hallinan, A. Minor, A. Hexemer and N. Balsara, *J. Electrochem. Soc.*, 2012, 159, A222-A227.
28. D. R. Ely and R. E. Garcia, *J. Electrochem. Soc.*, 2013, 160, A662-A668.
29. F. Ding, W. Xu, G. L. Graff, J. Zhang, M. Sushko, X. Chen, Y. Shao, M. H. Engelhard, Z. Nie and J. Xiao, *J. Am. Chem. Soc.*, 2013.
30. C. M. Lopez, J. T. Vaughey and D. W. Dees, *J. Electrochem. Soc.*, 2012, 159, A873-A886.
31. C. Monroe and J. Newman, *J. Electrochem. Soc.*, 2004, 151, A880-A886.
32. J. T. Vaughey, G. Liu and J. G. Zhang, *Mrs Bulletin*, 2014, 39, 429-435.
33. J. Steiger, D. Kramer and R. Moenig, *Electrochim. Acta*, 2014, 136, 529-536.
34. J. N. Chazalviel, *Phys. Rev. A*, 1990, 42, 7355-7367.
35. S. Schnur and A. Groß, *Catalysis Today*, 2011, 165, 129-137.
36. J. Steiger, G. Richter, M. Wenk, D. Kramer and R. Mönig, *Electrochem. Comm.*, 2015, 50, 11-14.
37. G. Richter, K. Hillerich, D. S. Gianola, R. Monig, O. Kraft and C. A. Volkert, *Nano Letters*, 2009, 9, 3048-3052.
38. M. Schamel, C. Schopf, D. Linsler, S. T. Haag, L. Hofacker, C. Kappel, H. P. Strunk and G. Richter, *Internat. J. Materials Res.*, 2011, 102, 828-836.
39. R. F. Sekerka, *Crystal Res. Technol.*, 2005, 40, 291-306.
40. Z. Li, J. Huang, B. Yann Liaw, V. Metzler and J. Zhang, *J. Power Sources*, 2014, 254, 168-182.
41. P. Novák, R. Imhof and O. Haas, *Electrochim. Acta*, 1999, 45, 351-367.
42. H. D. Yoo, I. Shterenberg, Y. Gofer, G. Gershinsky, N. Pour and D. Aurbach, *Energy & Environ. Sci.*, 2013, 6, 2265-2279.

43. M. Mohtadi and F. Mizuno, *Beilstein J. Nanotechnol.*, 2014, 5, 1291–1311.
44. T. J. Richardson and G. Chen, *J. Power Sources*, 2007, 174, 810-812.
45. C. Ling, D. Banerjee and M. Matsui, *Electrochim. Acta*, 2012, 76, 270-274.
46. A. Aryanfar, D. Brooks, B. V. Merinov, W. A. Goddard, A. J. Colussi and M. R. Hoffmann, *J. Phys. Chem. Lett.*, 2014, 5, 1721-1726.
47. J. W. Diggle, A. R. Despic and J. O. Bockris, *J. Electrochem. Soc.*, 1969, 116, 1503-&.
48. M. Z. Bazant, *Acc. Chem. Res.*, 2013, 46, 1144-1160.
49. Y. S. Cohen, Y. Cohen and D. Aurbach, *J. Phys. Chem. B*, 2000, 104, 12282-12291.
50. V. Fleury, *Nature*, 1997, 390, 145-148.
51. T. A. Witten and L. M. Sander, *Phys. Rev. Lett.*, 1981, 47, 1400-1403.
52. M. Jäckle and A. Groß, *J. Chem. Phys.*, 2014, 141, -.
53. T. M. Trimble and R. C. Cammarata, *Surface Sci.*, 2008, 602, 2339-2347.
54. A. Groß, *Theoretical Surface Science – A Microscopic Perspective*, Springer, Berlin, 2nd edn., 2009.
55. H. Brune, *Surf. Sci. Rep.*, 1998, 31, 125-229.
56. H. Jónsson, *Ann. Rev. Phys. Chem.*, 2000, 51, 623-653.
57. K. Doll, N. M. Harrison and V. R. Saunders, *J. Phys.-Condensed Matter*, 1999, 11, 5007-5019.
58. A. Aryanfar, US Patent App. 14/201,979, 2014.
59. A. Aryanfar, D. J. Brooks, A. J. Colussi and M. R. Hoffmann, *Phys. Chem. Chem. Phys.*, 2014, 16, 24965-24970.
60. K. Nishikawa, T. Mori, T. Nishida, Y. Fukunaka, M. Rosso and T. Homma, *J. Electrochem. Soc.*, 2010, 157, A1212-A1217.
61. F. P. Incropera and D. P. Dewitt, *Introduction to Heat Transfer*, Wiley, New York, N. Y., 6th edn., 2011.
62. P. K. Muhuri and D. K. Hazra, *Journal of Chemical and Engineering Data*, 1994, 39, 375-377.
63. K. A. Fichthorn and W. H. Weinberg, *J. Chem. Phys.*, 1991, 95, 1090-1096.
64. R. Akolkar, *J. Power Sources*, 2013, 232, 23-28.
65. S. Chandrashekar, N. M. Trease, H. J. Chang, L.-S. Du, C. P. Grey and A. Jerschow, *Nature Mat.*, 2012, 11, 311-315.
66. H. Brune, *Ann. Physik*, 2009, 18, 675-698.
67. C. M. Lopez, J. T. Vaughey and D. W. Dees, *J. Electrochem. Soc.*, 2009, 156, A726-A729.
68. C. Kittel, John Wiley & Sons, New York, 8th edn., 2004.
69. W. D. J. Callister and D. G. Rethwisch, *Fundamentals of materials science and engineering : an integrated approach*, Wiley, Hoboken, NJ, 4th edn., 2012.
70. A. Grazyna, *Surface diffusion : metals, metal atoms, and clusters*, Cambridge University Press, New York, N. Y., 2010.
71. E. G. Seebauer and C. E. Allen, *Progress Surf. Sci.*, 1995, 49, 265-330.
72. T. Alanissila and S. C. Ying, *Progress Surf. Sci.*, 1992, 39, 227-323.
73. D. A. Reed and G. Ehrlich, *Surf. Sci.*, 1981, 102, 588-609.
74. S. Y. Chang, C. E. Li, Y. C. Huang, H. F. Hsu, J. W. Yeh and S. J. Lin, *Scientific Reports*, 2014, 4.
75. L. P. H. Jeurgens, Z. M. Wang and E. J. Mittemeijer, *Int. J. Mat. Res.*, 2009, 100, 1281-1307.
76. J. Sun and S. L. Simon, *Thermochimica Acta*, 2007, 463, 32–40.
77. P. R. Couchman and W. A. Jesser, *Nature*, 1977, 269, 481-483.
78. L. W. Wang, *Philosophical Magazine*, 2013, 93, 3648-3663.
79. B. B. Alchagirov, L. K. Afaunova, F. F. Dyshekova, A. G. Mozgovoi, T. M. Taova and R. K. Arkhestov, *High Temperature*, 2009, 47, 287-291.
80. A. A. V. Grosse, *J. Inorg. Nucl. Chem.*, 1964, 26, 1349-1361.
81. *Atomic Defects in Metals*, Springer Berlin Heidelberg, 1991.
82. A. Aryanfar and e. al., *to be submitted*, 2015.
83. A. T. Ribes, P. Beaunier, P. Willmann and D. Lemordant, *J. Power Sources*, 1996, 58, 189-195.
84. Q. S. Mei and K. Lu, *Phil. Magazine Lett.*, 2008, 88, 203-211.
85. R. A. Huggins, *J. Power Sources*, 1999, 81, 13-19.



Lithium metal dendrite tips are shown to thermally relax into flatter domains over $\Delta E_R^\ddagger \sim 20 \text{ kJ mol}^{-1}$

barriers

GRAPHICAL ABSTRACT